Microbial Pb(II)-bioprecipitation: Characterising Responsible Biotransformation Mechanisms

Carla Cilliers[1], Olga Neveling[1], Shepherd M. Tichapondwa[1], Evans M. N. Chirwa[1] and Hendrik G. Brink*[1]

[1] Department of Chemical Engineering, Faculty of Engineering, Built Environment and Information Technology, University of Pretoria, Pretoria 0002, South Africa; u14053901@tuks.co.za (C.C.); u15037780@tuks.co.za (O.N.), shepherd.tichapondwa@up.ac.za (S.M.T), evans.chirwa@up.ac.za (E.M.N.C)
*Correspondence: deon.brink@up.ac.za

Abstract. The research aimed to facilitate the scalability of a lead bioremediation process through improved understanding of the dominant mechanisms present. The process utilises a local microbial consortium which previously demonstrated highly efficient bioremoval and -recovery of aqueous lead. To this end the project investigated lead bioremoval, microbial growth, and the effects of two different complementary anions (nitrates from lead nitrate and perchlorate from lead perchlorate) on the resulting precipitate composition and structure. The experiments were conducted anaerobically to facilitate dissimilatory metal reduction with Luria Bertani broth in the presence of different lead concentrations. Analyses included growth, lead removal, nitrate, perchlorate and sulphate measurements, transmission and scanning electron microscopy, X-ray diffraction, and energy-dispersive X-ray spectroscopy. A maximum lead removal rate of 4.71 ppm/h and a maximum specific growth rate of 0.76 μ/h were observed. Both the presence of nitrate, perchlorate, as well as different lead concentrations had significant effects on the precipitate. This contrasted with the growth that was solely affected by the lead concentrations present. Lead sulphide, elemental lead, elemental sulphur, and pyromorphite were present in the precipitate at varying ratios dependent on the conditions. The anoxic biotransformation of lead sulphide to pyromorphite was established, with the production of elemental sulphur in solid-state. A consistent amount of elemental lead was detected throughout, indicating dissimilatory reduction. A symbiotic relationship between sulphate reducing, lead reducing, sulphur oxidising, and denitrifying bacteria was found to be responsible for biotransformation and bioprecipitation. The improved understanding of the Pb bioremoval and bioprecipitation mechanisms presented in the current study provides much needed insights crucial to future scaling of the technology and consequent cleaner production of lead. To further elucidate the bioremediation processes involved in the system, it is recommended to conduct genomic and transcriptomic research into the microbiome to assess its adaptability under continuous operation.

Keywords: Bioremediation, biorecovery, lead, heavy metals.

1 Introduction

Lead (Pb) is a well-studied xenobiotic heavy metal that is biologically non-essential and non-degrading. Exposure to Pb poses several neurological dangers that include neurodevelopmental alterations and neurodegeneration (Lombó et al., 2017). Pb is known to intervene with the metabolism by disrupting crucial enzymes and bonding with biologically essential molecules (Rigoletto et al., 2020). In addition, Pb(II) poisoning can cause severe health complications including anaemia, diarrhoea, stomach ache, and kidney damage (Tao et al., 2020).

Pb is released into the environment predominantly through anthropogenic activities while a minimal contribution of natural sources has been reported. Lead can be naturally present in many mineral deposits (sediments that has economic potential) at concentrations ranging from 0.01 to 10 wt%, which is well above 5-80 ppm, but usually less than 20 ppm in areas that do not contain mineral deposits. However these deposits tend to be present in non-mobile mineral forms therefore limiting its bioavailability (Callender, 2005). Modern-day humans release Pb through Pb ore extraction and smelting, waste disposal, and the combustion of coal. A major contributing factor to lead pollution is the mining industry. It is reported that between 357 and 857 × 10^6 kg/y of lead is released into the environment per year due to mining and smelting activities. It is also estimated that 300 Mt of lead have been released into the environment as a result of lead ore processing in the past five millennia with the most released in the past 500 y (Zhang et al., 2012). A cleaner option for the production of Pb for industrial use is sought as the recovery and not only removal of Pb is of interest; it is estimated that *circa* 20 years' supply of raw Pb supply is available globally (Statista, 2019).

Conventional Pb(II) removal mechanisms include chemical precipitation, membrane filtration, electrolysis, ion exchange, or cementation (Pan et al., 2012; Tao et al., 2020). These methods tend to be expensive, complicated,

and likely to produce potential secondary pollution (Tao et al., 2020). Various studies have been conducted into Pb bioremediation as an environmentally friendly and cost-effective alternative, using a myriad of organisms such as plants (phytoremediation), fungi, or bacteria (Rigoletto et al., 2020).

The research conducted by this team has provided evidence of the effective removal and recovery of Pb(II) from solution and producing a precipitate that indicated the presence of elemental Pb and PbS (Brink et al., 2019). A second study was conducted to determine the effects of initial nutrient concentration on Pb(II) bioremoval, growth, nitrates, total organic carbon levels as well the consortium's population distribution. The species identified during Pb removal and recovery was *Clostridium bifermentans*, *Klebsiella pneumoniae*, *Listeria monocytogenes*, *Ralstonia solanacearum*, *Eneterococcus casseliflavus* as well as various uncultured species (Hörstmann et al., 2020). Pb(II) removal was not directly dependent on nitrate depletion and the microbial growth metabolism, indicating potential alternative Pb-removal mechanisms at work – possibly biosorption. However, it was shown that the effect of biosorption on Pb-removal by the consortium in question was negligible, eliminating this mechanism from the current investigation (Veenhuyzen et al., 2021). Continuous Pb removal was previously investigated (Chimhundi et al., 2021) and demonstrated the effective removal of Pb(II) in an upflow anaerobic sludge blanket (UASB) reactor. The reactor was capable of removing up to 2000 ppm Pb(II) with a maximum removal rate of 1948.4 mg/(L.d). However, limited understanding was presented on the Pb removal mechanism which consequently restricted the scalability of the system.

Theoretical Pb-removal by microbes in isolation have been extensively investigated, with the mechanisms commonly proposed for bioremoval of Pb mainly as biomineralization, intracellular accumulation, biosorption, and chelation with the aid of self-producing organic acids. Bacterial mechanisms specifically include precipitation of metals as sulphides, intracellular accumulation, biosorption, or encapsulation by excreted extracellular polymeric substances (Naik and Dubey, 2013). However, understanding of the relationship between different species of microbes within Pb-exposed communities and the consequent detoxification, metal resistance, and Pb-utilisation mechanisms resulting in overall survival is still sorely lacking in the literature.

The research gaps identified and subsequently addressed in the current study include the lack of knowledge on how the local Pb-resistant microbial consortium not only survive in extreme Pb contaminated conditions, but also biotransform and bioprecipitate Pb. Currently the dearth of information available on how such systems work limits the implementation on an industrial scale. The current study therefore aimed to give insight into the Pb-removal and Pb-precipitation mechanisms utilized by the consortium by studying the effects of Pb-concentration as well as the type of complementary anion (Nitrate or Perchlorate) used on the Pb-removal properties, consortial metabolic activities, culture medium ion compositions, precipitate morphologies, and crystalline compositions. The project ultimately aims to develop a scaled system for the cleaner production of Pb by facilitating the recovery of Pb from wastewater streams, therefore limiting the depletion of Pb reserves and harm to the environment.

2 Materials and Methods

2.1 Experimental Layout

Two sets of experiments were conducted, the first set was performed with only $Pb(NO_3)_2$ or $Pb(ClO_4)_2$ as stock solutions, spiked with approximately 80 ppm, 250 ppm and 500 ppm Pb(II) for a period of 42 h. Due to the hygroscopic nature of $Pb(NO_3)_2$ or $Pb(ClO_4)_2$, exact preparation of the stock solutions was not feasible and therefore the initial and final concentrations were consistently measured for all runs. The second set of experiments was conducted with $Pb(NO_3)_2$, $Pb(ClO_4)_2$ and a mixture of the two stock solutions for 5 d. The following schematic in **Fig. 1** depicts the experimental procedures. All graphs were created using *GraphPad Prism 9* software.

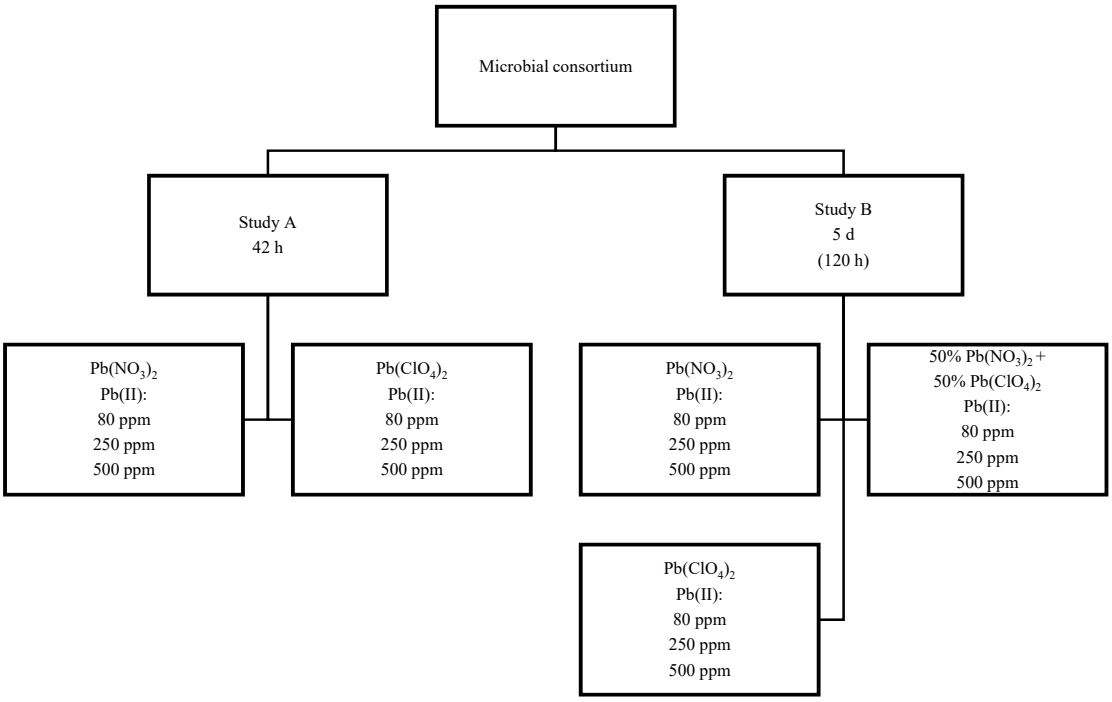

Fig. 1 Project layout

2.2 Microbial culture

The Pb(II) resistant microbial consortium was attained from a borehole at an automotive-battery recycling plant in Gauteng, South Africa (Brink et al., 2017). The initial inoculum was prepared by adding 1 g of Pb(II) contaminated soil to LB broth spiked with 80 ppm Pb(II) in a 100 mL anaerobic serum bottle, which was then incubated for 24 h and shaken at 32 °C and 120 rpm. The inoculum was cryogenically stored with glycerol at a final ratio of 20 % v/v at -77 °C. Precultures were prepared from the stored inoculum by inoculating 100 mL anaerobic serum bottles spiked with approximately 80 ppm, 250 ppm, and 500 ppm Pb(II). The serum bottles were sealed and incubated at 30 °C and shaken at 120 rpm until precipitation was visible. The new precultures were again cryogenically stored for direct inoculation of the experiments (Brink et al., 2019).

2.3 Materials

100 mL serum bottles were used to set up anaerobic batch reactors. Each reactor was spiked with a lead stock solution prepared with $Pb(NO_3)_2$ (Merck, Kennelworth, NJ). A mixture consisting of 10 g/L Tryptone, 5 g/L yeast extract and 1 g/L NaCl (Sigma Aldrich, St Louis, MO). Viable cell activity was measured at a wavelength of 550 nm using 3-(4,5-dimethylthiazol-2-yl)-2,5-diphenyl tetrazolium bromide (MTT) and dimethyl sulfoxide (DMSO) (Sigma Aldrich, St Louis, MO).

2.4 Experimental

The Pb(II) stock solution was added in a biological safety cabinet at the various concentrations to the growth medium after being autoclaved and cooled separately. The reactors were then inoculated with 0.2 ml of the previously stored precultures, purged with nitrogen gas for 3 min and sealed to create a strict anaerobic environment. The batch reactors were set up in triplicate and incubated at 35 °C and shaken at 120 rpm. An abiotic control experiment was carried out for a duration of 72 h to ensure that all conclusions and findings made were due to biological activity.

2.5 Sampling

Measurements were taken every 3 h for 42 h for Study A, with a hypodermic needle and sterile syringe by piercing the rubber stopper after ensuring that the reactors were shaken to obtain a homogenous mixture. In study B samples were taken every 24 h using the same method as for study A.

2.6 Analyses

2.6.1 Ion measurements

Pb(II), NO_3^-, ClO_4^-, PO_4^{-3} and Cl^- was measured with the aid of Ion Chromatography (IC). A 940 Professional IC vario ion chromatography (Metrohm, Herisau, Switzerland) with a Metrosep C 6–250/4.0 (Metrohm, Herisau, Switzerland) separation column and C 6- eluent- 8 mM oxalic acid (Metrohm, Herisau, Switzerland) was used. Pb(II), a transition metal, is not well detected by conductivity and therefore UV-Vis (Metrohm, Herisau, Switzerland) at a wavelength of 520 nm was used with a post-column reagent PAR (pyridylazoresorcinol: Thermo Fisher Scientific, Waltham, Massachusetts, United States) with HNO_3 (Glassworld, Robertville, Johannesburg, South Africa) and NH_4OH (25%) (Glassworld, Robertville, Johannesburg, South Africa).

2.6.2 Growth

Growth measurements were estimated using a metabolic activity assay which directly translates to cell viability. Metabolic activity is directly proportional to the metabolism which refers to the total of all chemical changes that take place in a cell to produce energy and basic materials required for important life processes (National Cancer Institute, 2022). Metabolic activity was measured immediately after sampling by determining the concentration of formazan crystals produced from yellow 3-(4,5-dimethylthiazol-2-yl)-2,5-diphenyl tetrazolium bromide (MTT: Sigma-Aldrich, Missouri, United States) by the action of the NADH-dependent cellular oxidoreductase enzyme (Wang et al., 2010). The formed formazan crystals were subsequently extracted using the organic solvent dimethyl sulfoxide (DMSO: Sigma-Aldrich, Missouri, United States) and the concentration measured spectrophotometrically at 550 nm (Brink et al., 2019). The wavelength of 550 nm was used as the original MTT stock solution is yellowish green of colour, but discolour to purple in the presence of viable cells and 550 nm is used to detect yellow green (Nassau, 1999).
Two measurements were taken of each sample, a measurement with biomass and measurement without; to eliminate background noise and act as a zero for quantification. The measurement without biomass was obtained by filtering each sample with 25 mm nylon syringe filters with 0.45 μm pores (Anatech, Olivedale, Johannesburg, South Africa). The pre-prepared MTT solution was then added to both the filtered and unfiltered samples and incubated for 60 min at 35 °C. The treated samples were subsequently dissolved using DMSO and their absorbance measurements were obtained to indicate cell viability.

2.6.3 Morphology and precipitate identity

Precipitate morphology was determined using both scanning and transmission electron microscopy (SEM and TEM). SEM was conducted on a Zeiss Ultra PLUS FEG scanning electron microscope coupled with energy-dispersive X-ray spectroscopy (EDS Oxford instruments, Aztec software, 20 kV) as well as a JEOL JEM 2100F for TEM. The remainder of each batch reactors were centrifuged for 10 min (21 ˚C) at 9000 rpm to obtain a solid pellet. These pellets were dehydrated and analysed using SEM and TEM. Precipitate identity was confirmed with X-Ray Diffraction (XRD) with an X-ray diffractometer (Rigaku Corporation, Tokyo, Japan) in conjunction with the results from SEM-EDS. The XRD-profiles were analysed using the X-ray diffraction software package *Match!3* (Crystal Impact GbR, Bonn, Germany) in conjunction with the freely available FullProf crystallographic software suite (Rodríguez-Carvajal, 1993). The FullProf suite facilitated Rietveld optimisation of the XRD phase identification (Ramkumar et al., 2018).

Mapping data was analysed by comparing each image on pixel scale. Mapping entails a high-resolution image of an area of interest that is collected alongside EDS data. The SEM microscope was adjusted at 20 kV. This interaction data was acquired using the software *ImageDiff* after normalizing against a monotone image. These monotone images were compared on pixel level to determine the number of corresponding sites and so the implied

interaction between the elements. The focus however was specifically on the relationship of the different elements to Pb and other relationships were not considered (de Wet and Brink, 2021).

3 Results

3.1 Study A

Study A was conducted over 42 h, the experiment was conducted in two runs to establish a continuous spectrum of measurements during the first 42 h, with either $Pb(NO_3)_2$ or $Pb(ClO_4)_2$ used as stock solution. Note that for simplification reasons, the reactors made with $Pb(NO_3)_2$ will be abbreviated at the end with an "N", reactors containing only $Pb(ClO_4)_2$ will be "C". The reactors are labelled as "A", which refers to study A, the spiked Pb(II) concentration followed by the Pb(II) stock solution used e.g. A80N: Study A, 80 ppm sample prepared with $Pb(NO_3)_2$.

3.1.1 Pb(II) removal, Metabolic Activity and Nitrate measurements

The Pb(II) measurements for 80 ppm, 250 ppm, and 500 ppm with $Pb(NO_3)_2$ and $Pb(ClO_4)_2$ for Run 1 and 2, are presented in **Fig. 2** (a-c). Note that the pastel-colored versions of each data set refer to the 2nd run for each global run. The Pb(II) measurements remained constant for first 4 h in all the reactors, followed by a drop and an increase and finally a drop again, suggesting a fast initial removal mechanism at work. This could possibly indicate an initial detoxification mechanisms in which a large fraction of the Pb(II) is initially immobilized prior to the partial liberation of Pb(II). Overall, the behaviour between samples containing $Pb(NO_3)_2$ and $Pb(ClO_4)_2$ were very similar in terms of lead removal – with a tendency towards a slightly higher Pb-removal in the $Pb(ClO_4)_2$ system.

The metabolic activity (MA) measurements for study A are presented in **Fig. 2** (d-f). The MA was stationary within the first 4 h, indicating a lag in growth for all three conditions. Similar trends were observed for the MA in the N and C runs for 80 ppm and 500 ppm Pb(II). However, significant differences in the N and C runs for the 250 ppm Pb(II) was measured. The MA values displayed a marked decrease for increasing Pb(II) concentration with final MA values in the 80 ppm Pb(II) runs measuring as high as 10 units, while the MA for 500 ppm measured around 2 units. Of particular interest was that the MA values measured in the A250N run resembled the MA measured in the 80 ppm Pb(II) while the MA in the A250C runs were closer to the 500 ppm Pb(II) runs.

The nitrate measurements for reactors containing $Pb(NO_3)_2$ are shown in **Fig. 2** (g-h). The data presented a dramatic drop in nitrates after 4 h to 6 h after the start of experiments for A80N and A250N, which directly corresponds to when growth was initiated. These results correspond with the measured MA values for the A80N and A250N runs and is further supported by previous work in which growth was shown to have a direct dependence on nitrate availability (Hörstmann et al., 2020). It was interesting to note that no drop in the nitrates in A500N. This suggests that a change in the consortial metabolism (likely due to a change in the consortial composition) in which nitrates are no longer utilized as terminal electron acceptor. This resulted in a decreased MA as observed in the 500 ppm Pb(II) runs. This same observation of difference in metabolism was likely responsible for the observed differences in the A250N and A250C runs. This observation does not provide complete clarity on the exact mechanism for Pb(II) removal as it related to the metabolism and therefore study B was performed.

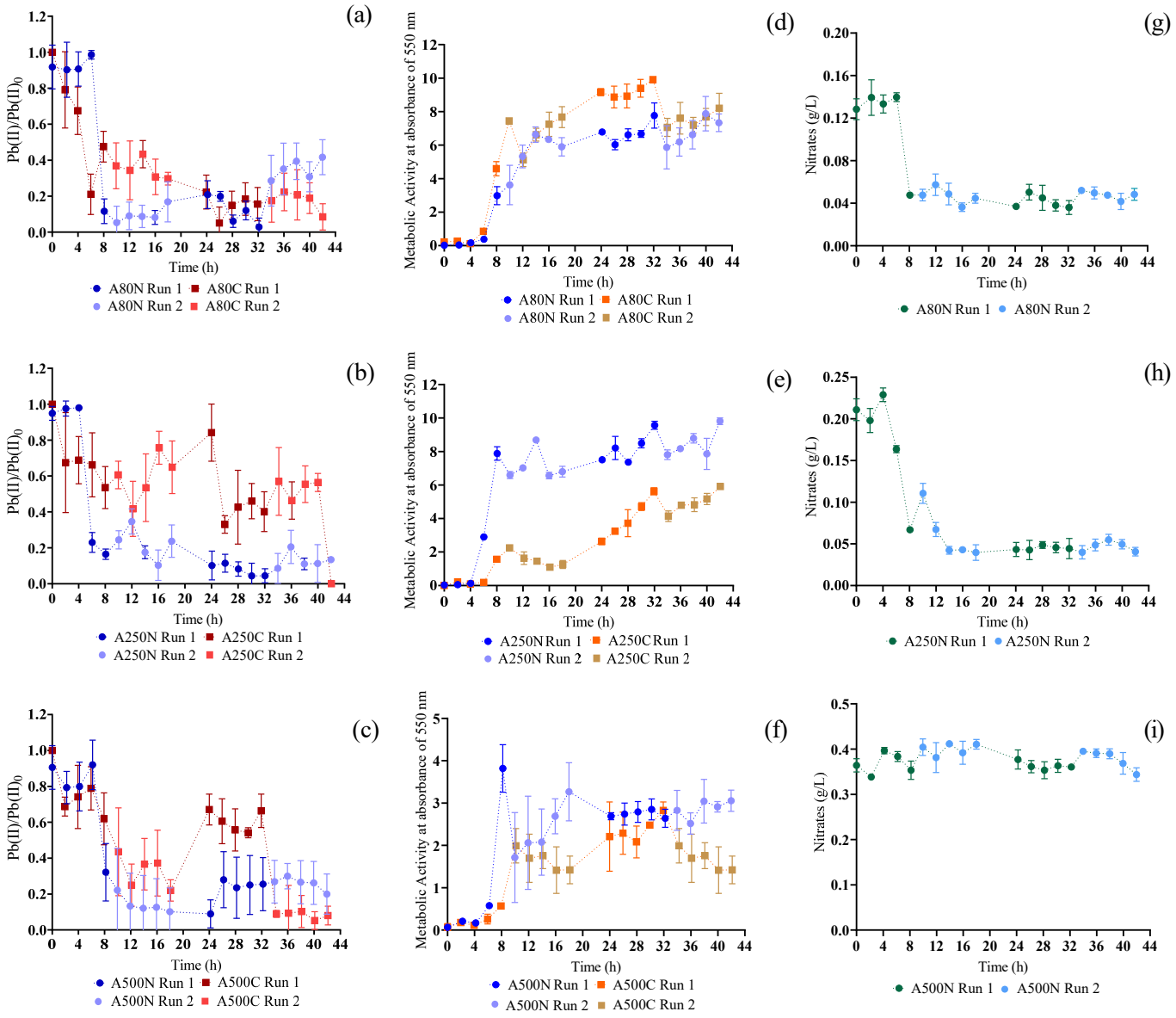

Fig. 2 Pb(II) removal for (a) A80N and A80C (b) A250N and A250C (c) A500N and A500C, metabolic activity for (d) A80N and A80C (e) A250N and A250C (f) A500N and A500C, and nitrate measurements for (d) A80N (e) A250N (f) A500N.

3.2 Study B

The second part of the study aimed to investigate the effects of nitrate (NO_3^-) and perchlorate (ClO_4^-) on lead bioremoval, growth, pH, ORP (oxidation-reduction potential), precipitate morphology and identification. Three different Pb(II) concentrations were tested with either 100 % $Pb(NO_3)_2$, a mixture of 50 % $Pb(NO_3)_2$ and 50 % $Pb(ClO_4)_2$ or 100 % $Pb(ClO_4)_2$. Same as previously used, reactors made with $Pb(NO_3)_2$ will be abbreviated at the end with an "N", reactors containing only $Pb(ClO_4)_2$ will be "C" and a mixture of the two will be "NC". The reactors are labelled as "B", which refers to study B, the spiked Pb(II) concentration followed by the Pb(II) stock solution used for example B80N for 80 ppm sample containing only $Pb(NO_3)_2$. The experiments were not conducted in triplicate, but with 500 mL batch reactors with the aim to produce as much possible precipitate for XRD analysis. It should be noted that study B is a lower resolution study on the process as compared to study A which focused on a finer grained experimental design used to identify the most pertinent questions to be answered.

Study A indicated the need to know more of the mechanisms involved in lead removal as well as the role of NO_3^- during Pb(II) removal under different conditions. Study B was conducted over 5 d to increase the amount of precipitate obtained.

3.2.1 Lead Removal

The change in lead removal for the second part of the study is presented in **Fig. 3**. The data from study A was added to the figures as individual data points to indicate the repeatability of the data gathered, bearing in mind the variability inherent in biological studies. The data generally followed the same trends as in study A, noting that study B was not an in-depth study and that more data points were generally gathered in study A. The data points for study A however do form an envelope around the data found in Study B, indicating repeatability. For the reactors containing 80 ppm Pb(II), it was found that final removal efficiencies of greater than 99 % were measured for all runs, except B250NC with > 80 % removal, after 5 d. Considering the difference between study A and B, no clear conclusion would be drawn regarding the Pb(II) removal efficiencies or -removal rates as a function of the Pb(II) concentrations or anion identities. This shows that the system is exceptionally robust in terms of overall Pb(II) removal for the studied conditions and medium compositions, which is consistent with previous results in which > 90 % Pb(II) removal of up to 2000 ppm Pb(II) was continuously achieved using the consortium under in question (Chimhundi et al., 2021).

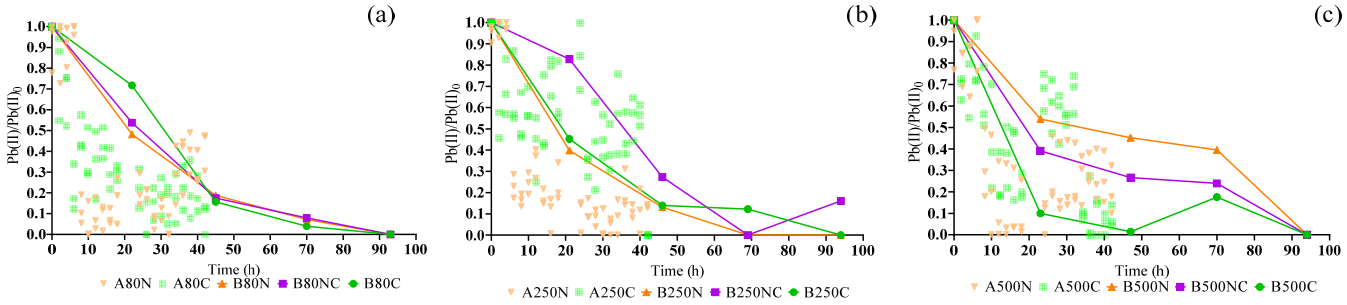

Fig. 3 The change in aqueous Lead for (a) A80N, A80C, B80N, B80NC and B80C (b) A250N, A250C, B250N, B250NC and B250C (c) A250N, A250C, B500N, B500NC and B500C.

3.2.2 Metabolic Activity Measurements

The Metabolic activity measurements for study B is presented in **Fig. 4** as well as the data found in study A. Repeatability was observed in the metabolic studies except for the comparison of A250N and B250N. The difference can be attributed to the slight variations in the initial Pb concentrations between A250N and B250N. Indicating that a point of growth inhibition of the nitrate reducing microbes were reached between the Pb(II) concentrations of 215 ppm (study A) and 288 ppm (study B).

From the figures below, it is observed that the lower concentrations of Pb(II) displayed overall higher growth measurements as opposed to samples containing 500 ppm Pb(II). Exponential growth within the first 24 h was much more apparent at 80 ppm, with a slight lag in the reactor containing $Pb(ClO_4)_2$. Overall it is observed that growth is slightly slower in the reactors containing $Pb(ClO_4)_2$, as opposed to the mixed or the $Pb(NO_3)_2$ reactors.

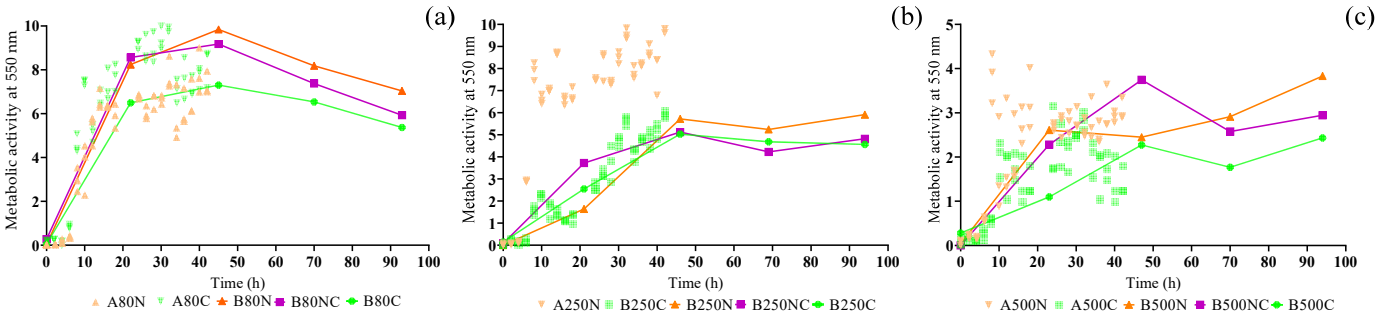

Fig. 4 Metabolic activity for (a) A80N, A80C, B80N, B80NC and B80C (b) A250N, A250C, B250N, B250NC and B250C (c) A250N, A250C, B500N, B500NC and B500C.

3.2.3 pH and ORP Measurements

The pH and ORP measurements for all runs are shown in **Fig. 5**. The drop in ORP measurements indicate that the systems were significantly reduced for the first 24 h for all experimental conditions.

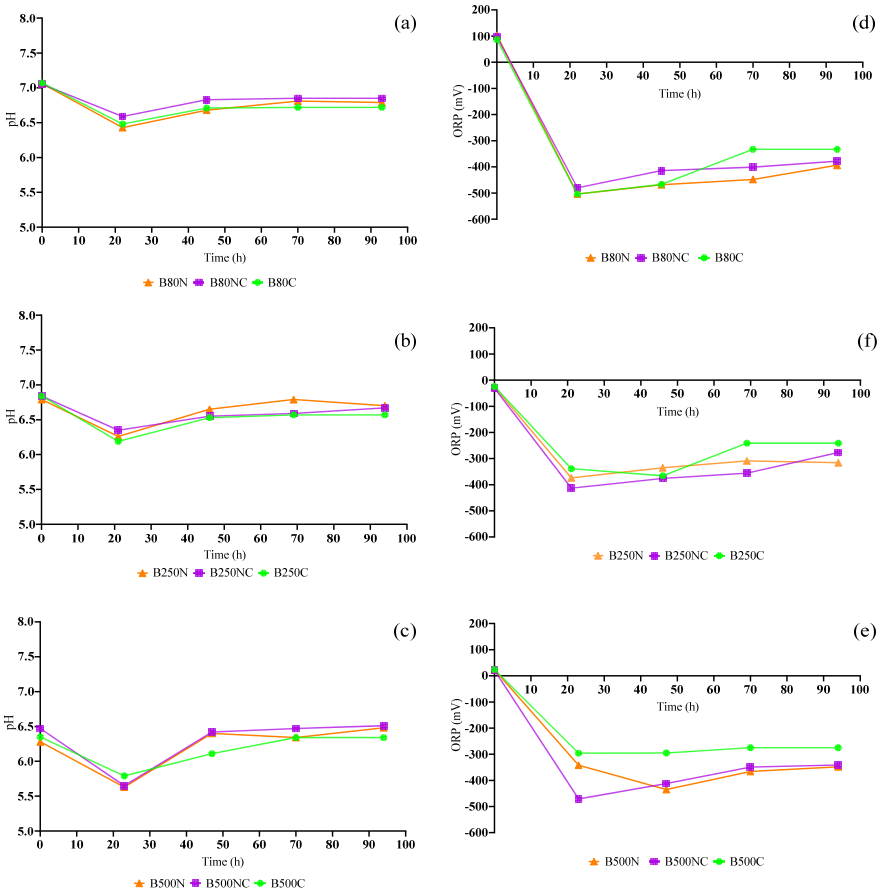

Fig. 5 (a) B80N, B80NC, B80C pH (b) B250N, B250NC, B250C pH (c) B500N, B500NC, B500C pH and (d) B80N, B80NC, B80C ORP (e) B250N, B250NC, B250C ORP (f) B500N, B500NC, B500C ORP.

It should be noted that the ORP values were the same for similar Pb(II) concentrations, indicating a strong correlation between the Pb(II) and ORP in the system. The drop in ORP was accompanied by a drop in the pH in

all the systems, which was followed by a steady increase to the original pH range. These results provide circumstantial evidence for the biological reduction of the Pb(II) in the solution for all conditions.

3.2.4 Anion measurements

The nitrate and perchlorate measurements are presented in **Fig. 6** and **Fig. 7**. The nitrates were depleted for both the lower two concentrations i.e. 80 ppm and 250 ppm as opposed to no nitrates being used at 500 ppm (correspondent to Study A). The sulphate measurements for B80 (all three runs) and B250N increased from 20 ppm to 80 ppm between 20 h – 40 h. B250NC and B250C exhibited increased sulphate measurements from 20 ppm to approximately 40 ppm over 5 d. The results for the perchlorate, phosphate and chloride measurements are reported in the Appendix A. These results indicate that negligible perchlorate was used in any of the experiments at any time. In addition, no clear conclusion could be drawn from the phosphate or chloride measurements for any of the runs.

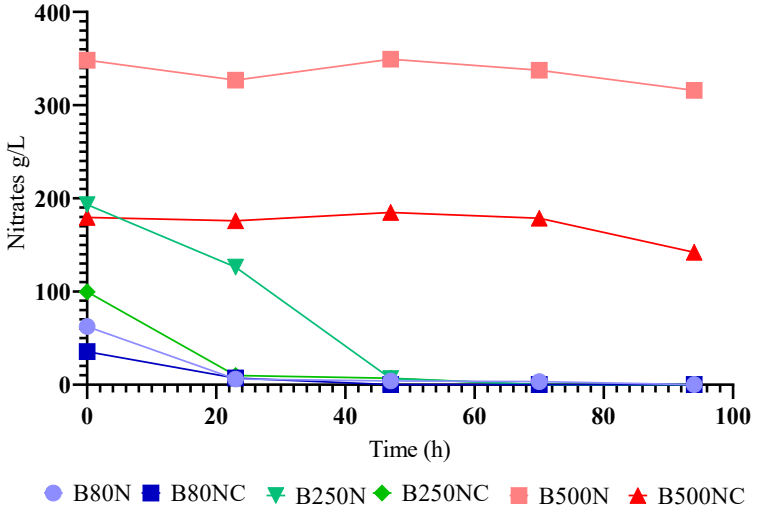

Fig. 6 Nitrate measurements at different concentrations of Pb(II) for study B.

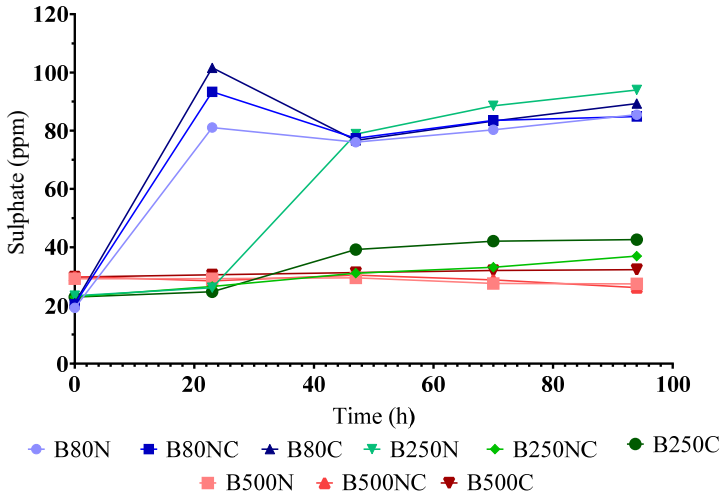

Fig. 7 Sulphate measurements at different concentrations of Pb(II) for study B.

3.2.5 SEM, TEM Images and EDS Mapping data

The SEM images for each condition is presented in **Fig. 8**. Different types of bacteria were visible from the images (same as study A) with spherical lead nanoparticles attached to the surface of the bacteria at the lower two

concentrations (80 ppm and 250 ppm) under all three conditions. The same spherical nanoparticles were observed in the 500 ppm samples but only with B500N and B500NC, as opposed to needle-like crystalline particles present in B500C. The B500N and B500NC samples presented a much more closely packed structure compared to the lower concentration samples.

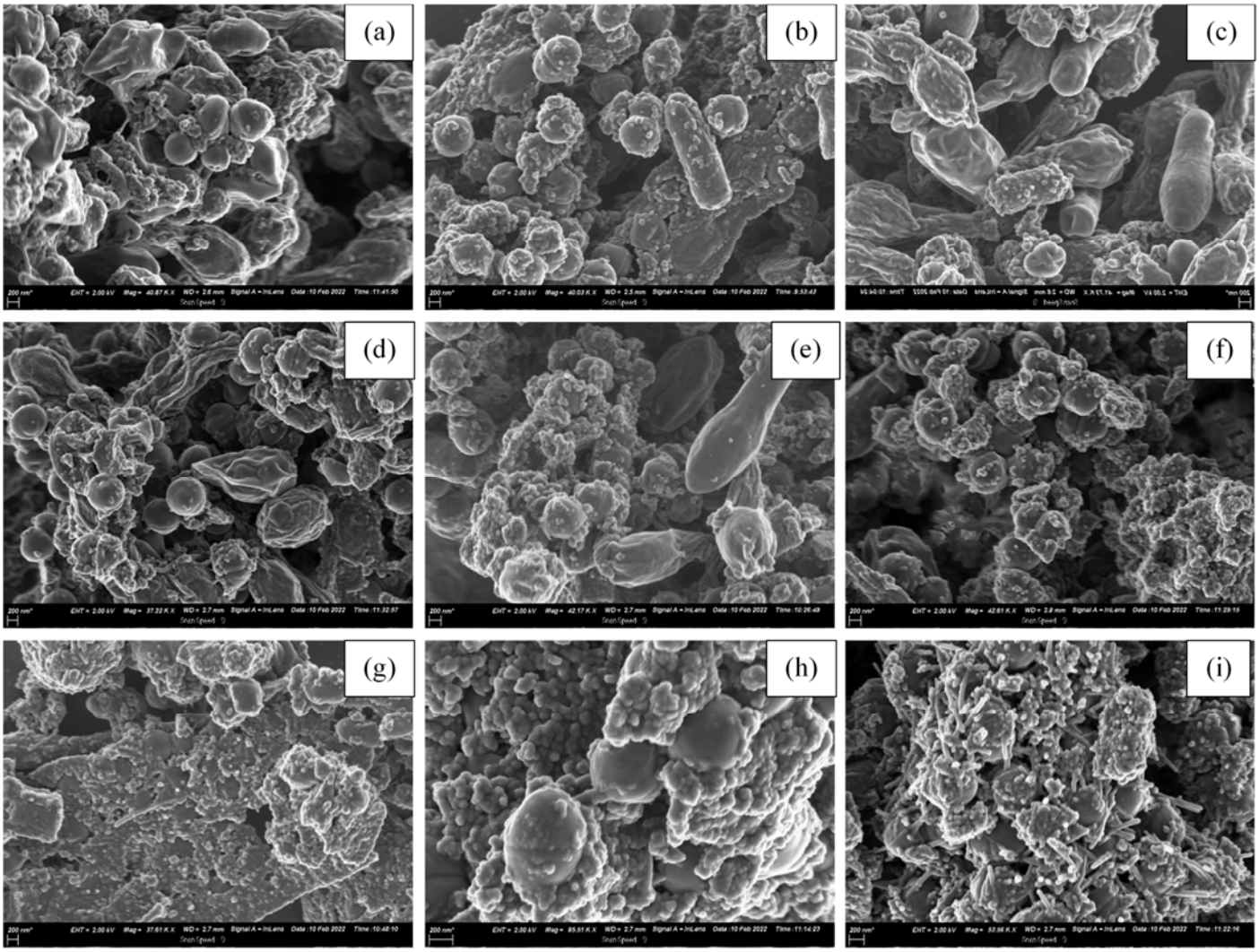

Fig. 8 SEM images of (a) B80N (b) B80NC (c) B80C (d) B250N (e) B250NC (f) B250C (g) B500N (h) B500NC (i) B500C.

The TEM images are presented in **Fig. 9**. The images found for B80 under all conditions presented spherical nanoparticles as precipitate on the outside of the cell walls, indicating extracellular precipitation. The 250 ppm samples presented similar nanoparticles as B80, but a few needle-like structures were visible as well. A few microbes presented precipitate on the inside of the cell walls at B250, which hinted at a small amount of intracellular precipitation. The B500 samples presented an increased amount of needle-like crystals corresponding with the SEM images for B500C. Most of the microbes had precipitate within the cell walls. An important observation, which couples with the SEM images, is that the B500 samples presented a considerably higher amount of needle like crystal structures as opposed to the other two conditions. These samples also showed various pockets of precipitate found on the inside of the cell wall at many sites in B500N, B500NC and B500C.

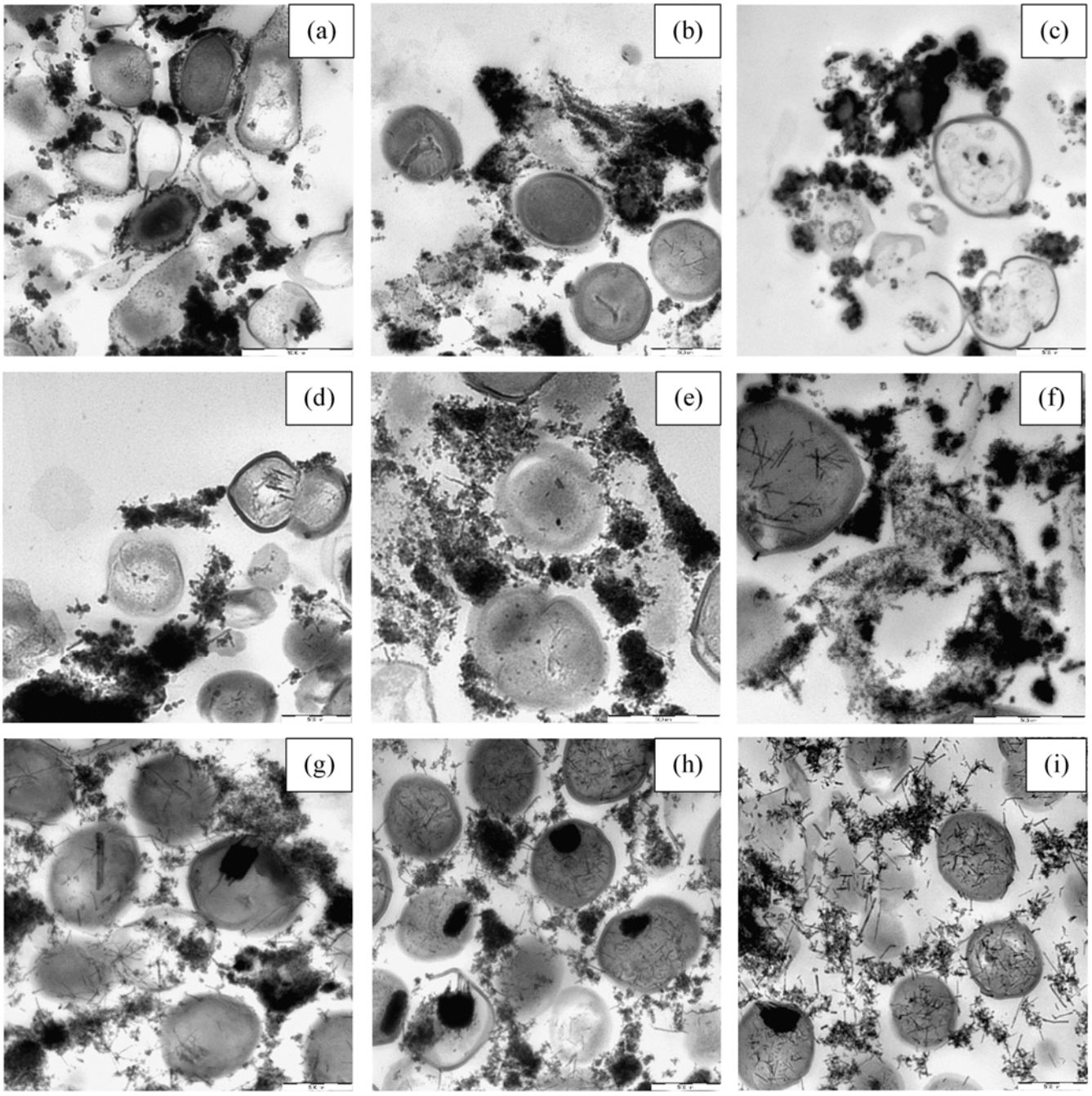

Fig. 9 TEM images of (a) B80N (b) B80NC (c) B80C (d) B250N (e) B250NC (f) B250C (g) B500N (h) B500NC (i) B500C.

3.2.6 SEM-EDS Elemental analysis

The SEM-EDS analysis is presented in **Fig. 10** as atomic ratios relative to the Pb fraction. The original SEM-EDS results indicated the predominant presence of oxygen in the precipitate of all the samples, followed by Pb. To improve the resolution of the results oxygen was disregarded to facilitate clarity. Phosphorous was found in B250 and B500 samples and a small amount in B80NC. The relationship between S and Pb in the B80 samples was 0.12:1 in B80N, 0.045:1 in B80NC, 0.26:1 in B80C. In the B250 samples 0.07:1 in B250N, 0.08:1 in B250NC and 0.06:1 in B250C. For the B500 a ratio of 0.05:1 in B500N, 0.07:1 in B500NC and 0.03:1 in B500C. Significantly high ratios of P to Pb was present in various of the samples, which can be attributed to the presence

of phosphate in the growth medium and in the biomass itself as well as an amount of Pb-P species to be investigated using XRD.

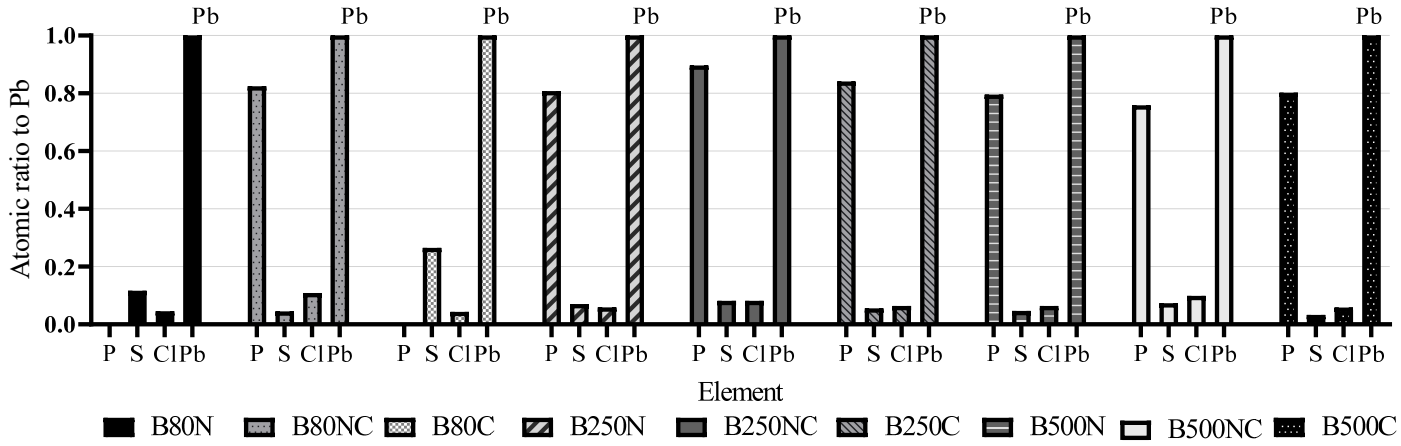

Fig. 10 Atomic ratios of each element with calculated with regards to Pb as detected by SEM-EDS analysis in each sample.

3.2.7 Mapping EDS

EDS Mapping analysis (comparison of Pb containing pixels to pixels occupied by other species) was conducted and presented in **Fig. 11**. The results indicate that lead has a high image correlation with all the elements (except P in the B80N and B80C runs). This indicates that the co-presence of S, O, Cl and P is expected in the precipitate, providing crucial information for the XRD precipitate analyses.

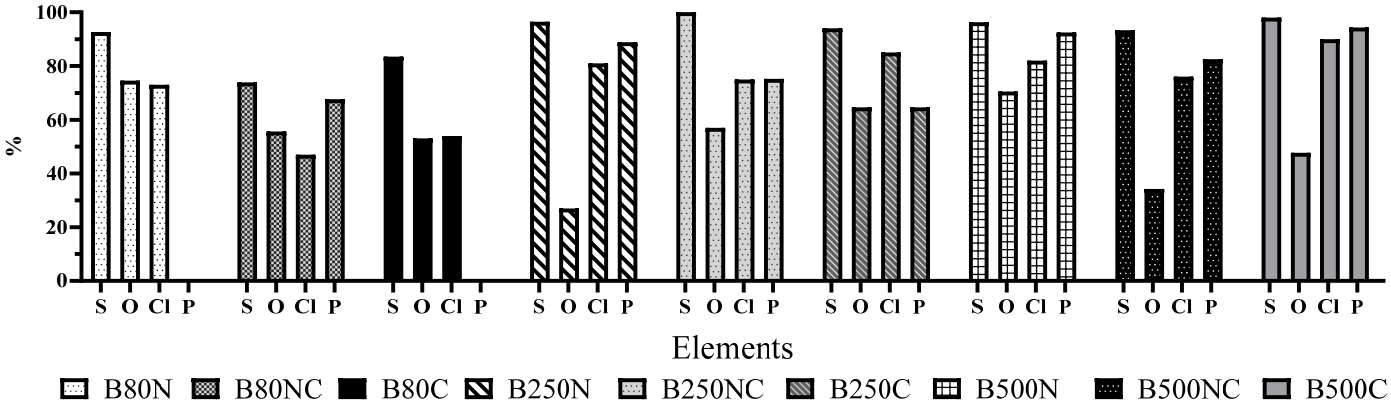

Fig. 11 Bar chart of the similarity between each element concerning Pb for all samples at B80, B250 and B500.

3.2.8 XRD Analysis

The XRD precipitate identification is presented in **Fig. 12** - **Fig. 14** for all conditions studied in part B. The results at each concentration are shown together in the figures below, but the separate spectra for each individual sample are reported in Appendix A. As discussed in the methods section, the XRD results were analysed using software *Match!3* coupled with Rietveld analysis using FullProf (Ramkumar et al., 2018). Four main components were identified in the precipitate under all conditions, namely elemental sulphur (S_{16}), lead sulphide (PbS), pyromorphite ($Pb_5(PO_4)_3Cl$) and elemental lead (Pb^0). The prominent species found in all reactors were PbS and $Pb_5(PO_4)_3Cl$. **Table 1** presents the results analysed using the Rietveld method for quantitative XRD analysis

(Gualtieri et al., 2019), presenting the mass fractions of each species in the precipitate. The results conducted on molecular basis are presented in the Appendix A.

Higher amounts of $Pb_5(PO_4)_3Cl$ were present in the samples containing 250 ppm and 500 ppm Pb(II) compared to PbS (**Table 1**) with fractions varying between 52.1 % and 78.0 %. As opposed to PbS being the predominant species at 80 ppm Pb(II) with fractions of between 49.5 % and 63.0 %. Pb^0 was consistently present in all samples, indicating a small amount of Pb(II) used as terminal electron acceptor as opposed to any of the anions present.

From literature, it was found that PbS presents spherical nanoparticles using SEM (Karami et al., 2013) as opposed to $Pb_5(PO_4)_3Cl$ which is of crystal nature (Topolska et al., 2013). This corresponds to the findings obtained for SEM and TEM analysis, as the highest ratio of $Pb_5(PO_4)_3Cl$ was found at higher Pb(II) concentrations.

It was established in a study conducted by Walczak et. al. that the biotransformation of PbS to pyromorphite ($Pb_5(PO_4)_3Cl$) was possible under oxic conditions, resulting in the oxidation of sulphide and the formation of elemental sulphur. The same study found that elemental sulphur was present in the solid phase and a small amount of sulphur was as sulphide and thiosulphate in solution. These findings explain how $Pb_5(PO_4)_3Cl$ came to exist from samples containing PbS. The phosphorus needed for this process can be obtained from phosphorus present in the LB broth supplemented to the reactors. There was also elemental sulphur present in the XRD results, corresponding to that found in literature. It should also be noted that this system is not oxic, but rather anoxic, due to the presence of bonded oxygen either NO_3^- or ClO_4^- or in the growth medium itself. Indicating that biotransformation of PbS to $Pb_5(PO_4)_3Cl$ is possible under anoxic conditions.

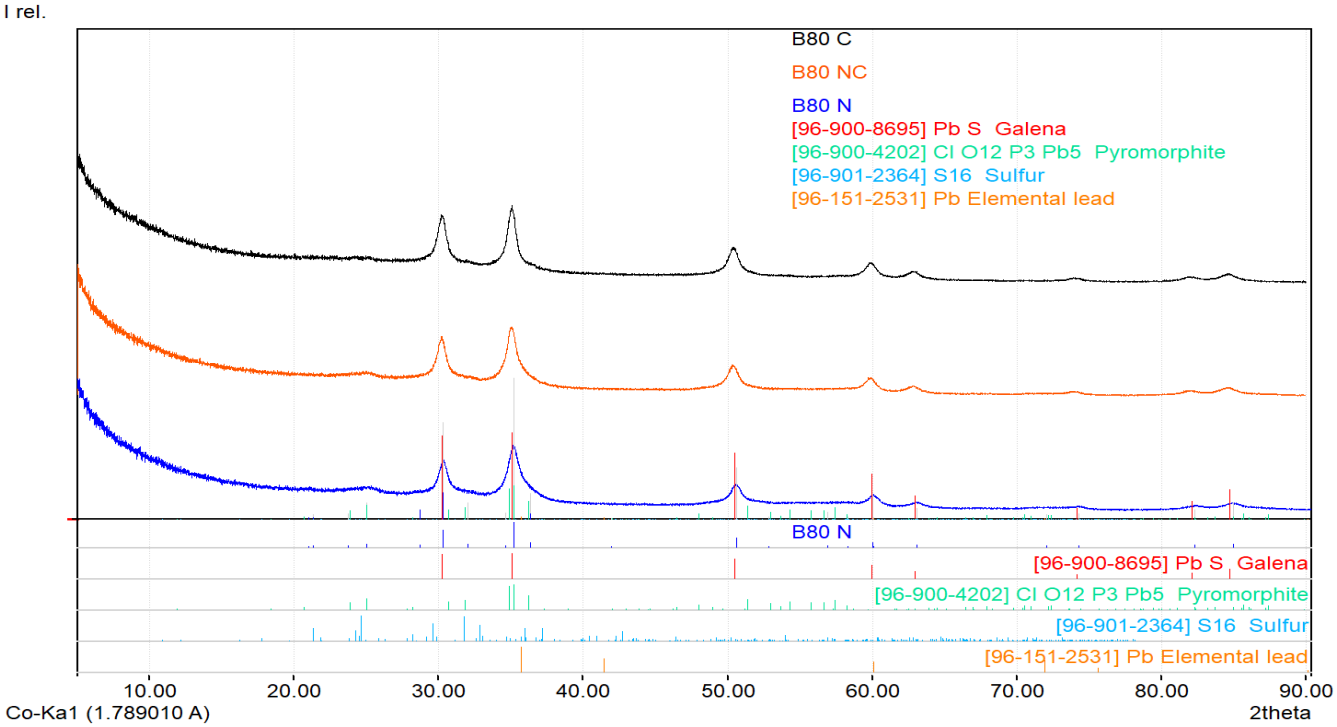

Fig. 12 XRD results for all three B80 samples.

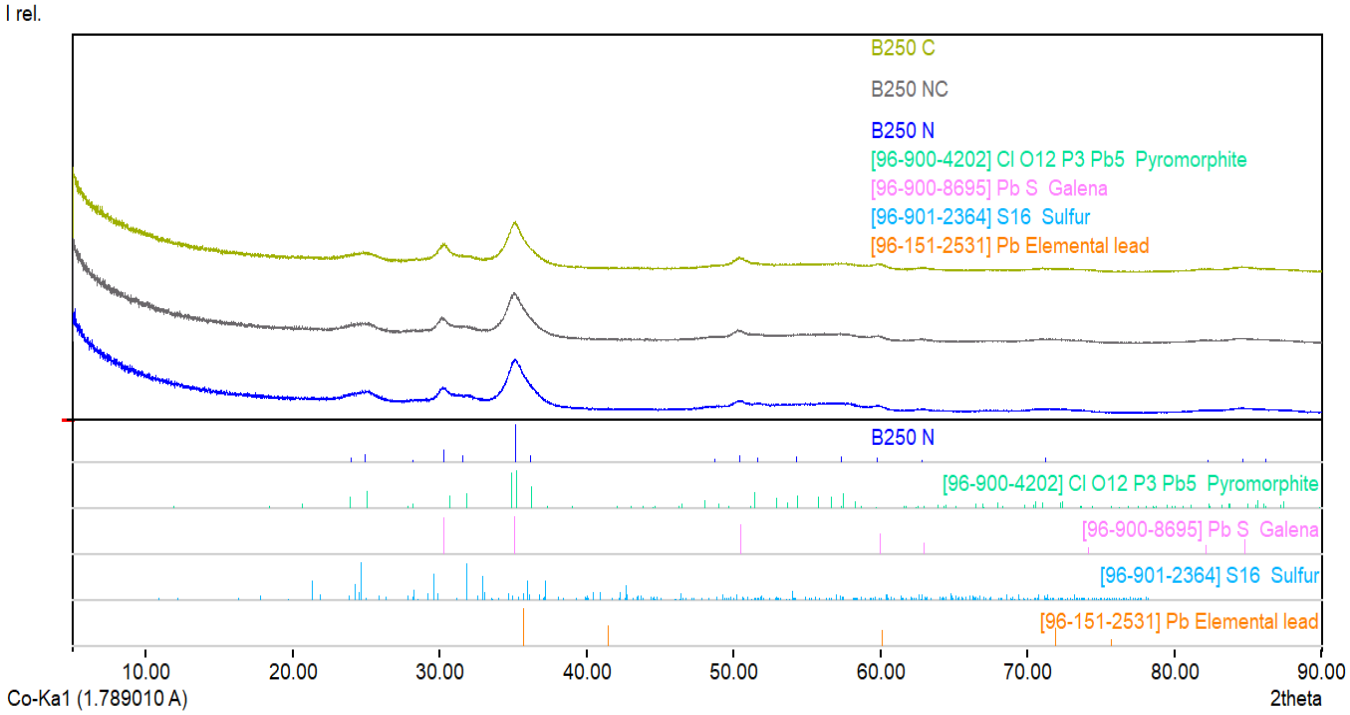

Fig. 13 XRD results for all three B250 samples.

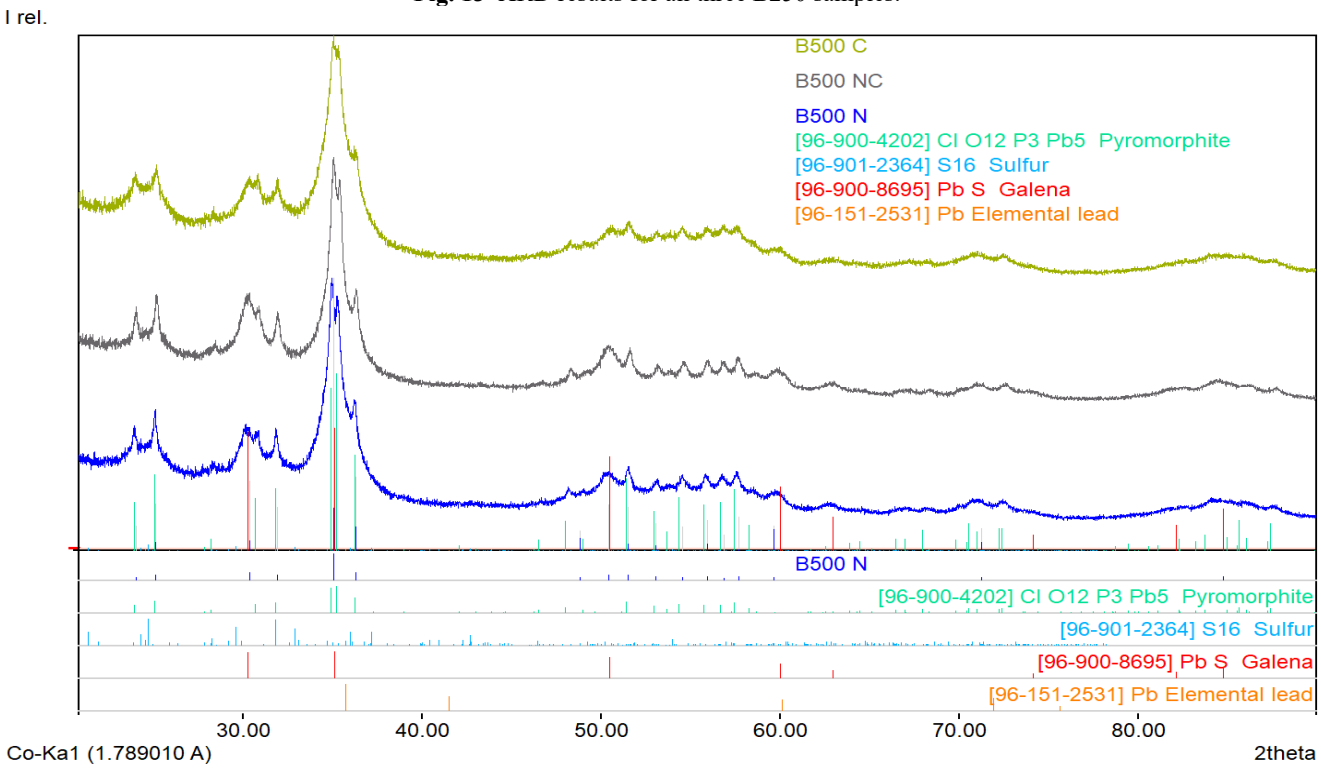

Fig. 14 XRD results for all three B500 samples.

Table 1 XRD results for each of the Pb species detected shown as fractions of a whole with the Rietveld chi-squared for each analysis.

Run	Pb^0 %	PbS %	Pyromorphite ($Pb_5(PO_4)_3Cl$) %	S_{16} %	χ^2
B80N	2.6	49.5	40.3	7.6	3.4
B80NC	2.8	63.0	32.0	2.3	3.3
B80C	1.7	62.4	22.1	13.9	6.1
B250N	6	20.3	57.5	16.3	9.9
B250NC	3.9	28.0	58.7	9.4	8.1
B250C	1.9	30.7	52.1	15.3	8.6
B500N	1.1	15.9	78.0	5.0	6.7
B500NC	1.3	30.8	53.1	11.5	7.2
B500C	2.9	12.1	55.6	29.4	5.8

3.2.9 Mass requirements

The findings revealed the presence of 4 prominent compounds present in the precipitate with Pb^0, S_{16}, PbS and $Pb_5(PO_4)_3Cl$. The theoretical amounts of each element needed to produce each component for 1 g precipitate to be produced was calculated in **Table 2**. The aim was to determine if the concentrations measured with ion chromatography was correspondent to the results obtained with XRD analysis. The XRD ratios between each component was used and added to a total of 100 (for XRD %) and converted to a total of a 1 g of precipitate as XRD is measured on a mass basis (Stutzman et al., 2016). Note that the phosphate and chloride measurements were also obtained using ion chromatography, the data obtained is however reported in Appendix A. The initial phosphate measurements obtained were significant, ranging between 363 ppm and 595 ppm. No apparent trend was established from these measurements as no clear increase or decrease was observed in the reactors. The data below however suggest that the concentration of phosphate required to produce the different amounts of $Pb_5(PO_4)_3Cl$ are comparably small to the initial concentration available in all the reactors. The same lack in trend was observed in the chloride readings, with no major change. The initial readings were similar for all the reactors ranging from 713 ppm to 737 ppm. The amount of chloride necessary for each of the reactors are insignificant compared to the initial concentration of chloride available. Both these results indicate that a substantial change due to precipitate requirements in either the phosphate or chloride readings would not be observed in the IC readings.

Table 2 Mass requirements with respect to the XRD results.

Element	B80N	B80NC	B80C	B250N	B250NC	B250C	B500N	B500NC	B500C
					(g/g)				
Pb	0.76	0.82	0.73	0.68	0.73	0.68	0.74	0.69	0.56
S	0.14	0.11	0.02	0.19	0.13	0.19	0.07	0.16	0.31
PO_4	0.08	0.07	0.05	0.12	0.12	0.11	0.16	0.11	0.12
Cl	0.01	0.01	0.01	0.02	0.02	0.01	0.02	0.01	0.01

4 Discussion

4.1 Lead removal and growth rates

The lead removal and specific growth rates for the different experimental conditions are reported in **Table 3**. The rates of lead removal were calculated as the change in concentration (ppm) over time and specific growth rates were calculated by dividing the first derivative with time (h) of the metabolic activity curve by the metabolic activity at that time – see **Equation 1** (Hörstmann et al., 2020).

$$\mu = {dX}/{dt\,\frac{1}{X}} \quad (1)$$

X: Metabolic activity at the time
μ: Specific growth rate

An excess of substrate is assumed with μ_{max} equal to μ. The highest Pb(II) removal rate in Study A was found in A500C (4.71 ppm/h). The samples containing perchlorate exhibited overall a higher measurement of lead removal. Study B exhibited overall lower lead removal measurements, which corresponds with less "fine-grain" sampling intervals when compared with Study A. The specific growth measurements indicated a maximum in A250N samples and overall higher measurements in samples containing nitrates. Indicating that lead removal was not growth dependent.

Table 3 Lead removal and specific growth rates for Study A and Study B

Study	Run	Average Pb(II) removal rate ppm/h	Specific growth rate μ_{max}/h
Study A	A80C	0.67	0.38
	A80N	0.24	0.60
	A250C	1.87	0.25
	A250N	1.07	0.76
	A500C	4.71	0.51
	A500N	2.25	0.51
Study B	B80N	0.59	0.23
	B80NC	0.54	0.16
	B80C	0.37	0.22
	B250N	1.30	0.35
	B250NC	0.96	0.18
	B250C	1.49	0.14
	B500N	1.79	0.18
	B500NC	2.46	0.34
	B500C	3.43	0.06

4.2 Background on microbial Mechanisms

Known microbial metabolic and detoxifying mechanisms involving Pb include anaerobic denitrification, sulphur oxidation, and biotransformation (Naik and Dubey, 2013). Anaerobic denitrification is the respiration process where nitrate is reduced to gaseous nitrogen forms. Nitrate acts as terminal electron acceptor with the help of dissimilatory enzyme nitrate reductase (Cathrine and Raghukumar, 2009). Nitrate reductase is also known to release sulphur during anaerobic denitrification (Cerqueira et al., 2009).
Microbial sulphur oxidation is the process where various inorganic sulphur compounds such as sulphide or elemental sulphur are oxidized with the reduction of oxygen (aerobic conditions) or an alternative electron acceptor (e.g. nitrate – NO_3^-) under anoxic conditions (Jost et al., 2010).
The biotransformation of PbS to pyromorphite have been shown under oxic abiotic conditions using a chemoautotrophic organism *Bosea* sp. Biotransformation of PbS to $Pb_5(PO_4)_3Cl$ (pyromorphite) is the process during which phosphates and chlorides reacts biologically with PbS resulting in the formation of elemental sulphur, sulfate, and pyromorphite (Walczak et al., 2016).

4.3 Responsible microbial Mechanisms

The usage of nitrates was most prominent at lower concentrations of Pb(II) (80 ppm and 250 ppm) but the lack thereof at low concentrations do not considerably inhibit growth or lead removal. This observation is attributed to the presence of more than one microbial culture present in the consortium. The presence of more than one culture as well as their identities were confirmed in a previously published article by this team in 2020 on the same microbial consortium as described in this study (Hörstmann et al., 2020) in which a change in community prevalence was confirmed at different concentrations of Pb(II). The presence of many species was detected including *Clostridium bifermentans*, *Klebsiella pneumoniae*, *Listeria monocytogenes*, *Ralstonia solanacearum*, *Eneterococcus casseliflavus* and various uncultured species were observed in the consortium. Both *Klebsiella pneumoniae* and *Ralstonia solanacearum* are well-known sulphate reducing (Holmes et al., 1997), sulphur oxidizing (Behera et al., 2016; Fazzini et al., 2013) and denitrifying bacteria (Dalsing et al., 2015; Zhang et al., 2018). The current findings substantiate the presence of the denitrifying microbes in the culture, but that these cultures are most likely not responsible for Pb(II) removal. The lack of nitrate usage at higher concentrations of Pb(II) indicates that these denitrifiers are not part of the highly Pb(II) resistant community and further supports the observation that these species are likely not responsible for Pb(II) removal as the Pb(II) removal was not significantly inhibited by their absence. The difference in TEM and SEM findings at different Pb(II)

concentrations was significant as it showed that Pb(II) was precipitated extracellularly at 80 ppm Pb(II) as opposed to evidence of intracellular precipitation at 250 ppm and 500 ppm Pb(II). The higher concentration samples presented crystalline precipitate as well as spherical nano-particles, compared to the lower concentrations presenting predominantly spherical nanoparticles. From literature is evident that the intercellular behavior can be attributed to the production of Metallothionein which are low molecular weight metal-bonding proteins with a high cysteine content in which the thiol group of cysteine is responsible for a high affinity towards heavy metals. These proteins are responsible for intracellular lead sequestration as well as transportation, storage and the detoxification of lead. Metallothionein-producing bacteria are resistant to high concentrations of lead and would explain the phenomenon only occurring at increased Pb(II) concentrations (Sevak et al., 2021).

The results obtained with XRD analyses directly corresponded with the data gathered during SEM-EDS mapping as well as the EDS data. Four compounds were identified with XRD analysis, namely pyromorphite, lead sulphide, elemental lead and elemental sulphur. A large amount of Pb corresponded with the exact sites where sulphur, phosphorous and chlorine were present, indicating that the majority of Pb was present as PbS or Pyromorphite. The crystalline particles at higher concentrations correspond to the higher presence of pyromorphite at higher Pb(II) concentrations (Manecki et al., 2006). It was established that there are sufficient amounts of each element or ion available in the systems to sustain the formation of the four compounds in the amounts determined by XRD analyses.

The existence of Pyromorphite ($Pb_5(PO_4)_3Cl$) was attributed to the biotransformation of PbS to Pyromorphite under anoxic conditions. Smaller amounts of Pyromorphite detected at 80 ppm Pb(II) could be due to the change in active species at different Pb(II) concentrations i.e. the presence of denitrifiers at lower concentrations resulting in higher amounts of sulphur release via the enzyme nitrate reductase (Cerqueira et al., 2009). A schematic of the proposed lead removal mechanisms is presented in **Fig. 15**. The active presence and lead resistance of denitrifying bacteria, sulphur oxidizing bacteria, a sulphur reducing bacteria as well lead reducing bacteria were established. The mechanisms in **Fig. 15**, with (a and d) the release of sulphur with the available sulphur reducing and denitrifying bacteria (only at lower Pb(II) concentrations), resulting in the formation of PbS (b). The PbS is in turn biotransformed to pyromorphite with the formation of elemental sulphur and release of SO_4^{2-} with Sulphur oxidizing bacteria (c). The occurrence of Pb^0 was formed with the aid of Lead reducing bacteria (e) from Pb(II). The exact identities of the lead reducing bacteria is unknown for the current consortium and it is recommended to establish their identities with a comprehensive study of the microbiome itself using 16S-rDNA analysis and other relevant metagenomic analysis.

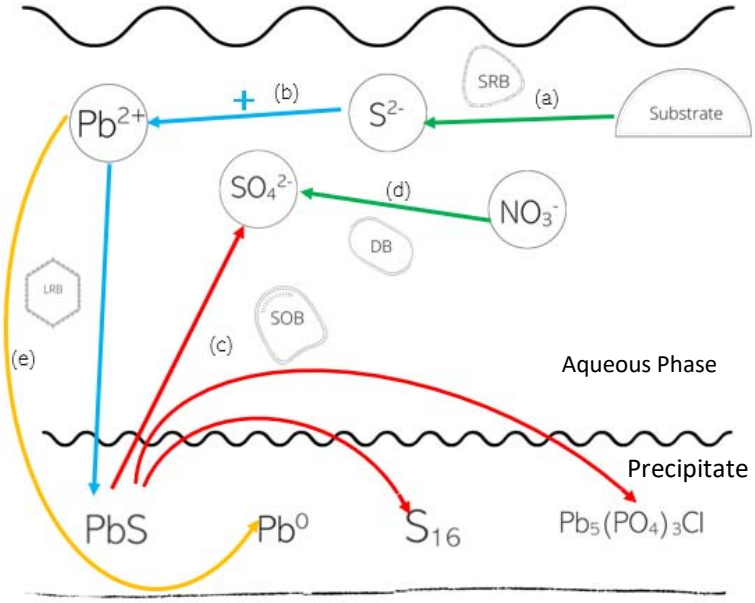

Fig. 15 A visual explanation for the microbial lead removal and recovery mechanisms. Abbreviations: SRB: Sulphate reducing bacteria, LRB: Lead reducing bacteria, SOB: Sulphur oxidizing bacterial, DB: Denitrifying bacteria.

5 Conclusion

This novel study investigated the importance of different Pb(II) concentrations and anions on microbial growth, lead removal, and precipitate composition and identification. The study proved that the microbial culture is robust in its ability to remove Pb(II) from solution under varying operational conditions. The different species of lead as well as the use and non-use of certain anions was attributed to the different roles of cultures in the consortium. This is the first study to investigate the effect of perchlorate on Pb(II) removal as well as the first to compare these results to that of nitrate, as well as the first study to prove the biotransformation of PbS to pyromorphite possible under anoxic conditions. The results indicate the successful co-existence of different microbial cultures and their various contributions to Pb(II) removal and final precipitate identity.

The findings presented facilitates the implementation of a cleaner method of Pb production due to the improved understanding provided on the precipitate identity and the response of the mixed microbial culture to the culture conditions. The study provides greater insight and understanding of the different mechanisms at work in a mixed industrial microbial community, providing a foundation for future research to be conducted on the industrial scaling and optimization of elemental Pb recovery using the local South-African microbial consortium.

Prior to implementation it is recommended that the temporal effects of different operational conditions (Pb concentrations, hydraulic residence times, startup procedure) on the Pb removal process as well as the genomic and transcriptomic response of the microbiome itself be undertaken.

Funding and declarations: This work is based on the research supported in part by the National Research Foundation of South Africa (Grant Numbers 120321, 145848, 121891 and 128088).

All authors certify that they have no affiliations with or involvement in any organization or entity with any financial interest or non-financial interest in the subject matter or materials discussed in this manuscript.

All authors contributed to the study conception and design. Conceptualization: Carla Cilliers, Hendrik G. Brink; Methodology: Carla Cilliers, Hendrik G. Brink; Formal analysis and investigation: Carla Cilliers, Olga Neveling; Writing - original draft preparation: Carla Cilliers, Hendrik G. Brink; Writing - review and editing: Carla Cilliers, Olga Neveling, Shepherd M. Tichapondwa, Evans M.N. Chirwa, Hendrik G. Brink; Funding acquisition: Evans M.N. Chirwa, Hendrik G. Brink; Supervision: Evans M. N. Chirwa, Hendrik G. Brink. All authors commented on previous versions of the manuscript. All authors read and approved the final manuscript.

Data availability: The datasets generated during and/or analysed during the current study are available from the corresponding author on reasonable request

References

Behera, B.C., Singh, S.K., Mishra, R.R., Thatoi, H., 2016. Partial Purification and Characterisation of Sulphur Oxidase from Micrococcus sp. and Klebsiella sp. Isolated from Mangrove Soils of Mahanadi River delta, Odisha, India. https://doi.org/10.13189/ujmr.2016.040302.

Brink, H.G., Hörstmann, C., Peens, J., 2019. Microbial Pb(II)-precipitation: the influence of oxygen on Pb(II)-removal from aqueous environment and the resulting precipitate identity. Int. J. Environ. Sci. Technol. 17, 409–420. https://doi.org/10.1007/s13762-019-02502-4.

Brink, H.G., Lategan, M., Naudé, K., Chirwa, E.M.N., 2017. Lead removal using industrially sourced consortia: Influence of lead and glucose concentrations. Chemical Engineering Transactions. https://doi.org/10.3303/CET1757069.

Callender, E., 2005. Heavy Metals in the Environment — Historical Trends. Environ. Geochemistry 9.

Cathrine, S.J., Raghukumar, C., 2009. Anaerobic denitrification in fungi from the coastal marine sediments off Goa , India. Mycol. Res. 113, 100–109. https://doi.org/10.1016/j.mycres.2008.08.009.

Cerqueira, N.M.F.S.A., Gonzalez, P.J., Brondino, C.D., Roma, M.J., Moura, I., Moura, J.J.G., Lisboa, U.N. De, Cie, F. De, Lisboa, U.N. De, 2009. The Effect of the Sixth Sulfur Ligand in the Catalytic Mechanism of Periplasmic Nitrate Reductase. https://doi.org/10.1002/jcc.

Chimhundi, J., Horstmann, C., Chirwa, E.M.N., Brink, H.G., 2021. Microbial Removal of Pb(II) Using an Upflow Anaerobic Sludge Blanket (UASB) Reactor. Catalysts 11, 512. https://doi.org/10.3390/catal11040512

Dalsing, B.L., Truchon, A.N., Gonzalez-Orta, E.T., Milling, A.S., Allen, C., 2015. Ralstonia solanacearum Uses Inorganic Nitrogen Metabolism for Virulence, ATP Production, and Detoxification in the Oxygen-Limited. MBio 6, 1–13. https://doi.org/10.1128/mBio.02471-14.

de Wet, M.M.M., Brink, H.G., 2021. Lead biosorption characterisation of aspergillus piperis. Sustain. 13. https://doi.org/10.3390/su132313169.

Fazzini, R., Cortes, M.P., Padilla, L., Daniel, M., Marko, B., Alejandro, M., Pilar, P., 2013. Stoichiometric Modeling of Oxidation of Reduced Inorganic Sulfur Compounds (Riscs) in Acidithiobacillus thiooxidans 110, 2242–2251. https://doi.org/10.1002/bit.24875.

Gualtieri, F.A., Gatta, D.G., Arletti, R., Artioli, G., Ballirano, P., Cruciani, G., Guagliardi, A., Malferrari, D., Masciocchi, N., Scardi, P., 2019. Quantitative phase analysis using the Rietveld method: towards a procedure for checking the reliability and quality of the results Quantitative phase analysis using the Rietveld method: towards a procedure for checking the reliability and quality of the. An Int. J. Mineral. Crystallogr. Geochemistry 88, 147–151. https://doi.org/10.2451/2019PM870.

Holmes, J.D., Richardson, D.J., Saed, S., Evans-, R., Russell, D.A., Sodeau, J.R., 1997. Cadmium-specific formation of metal sulfide Q-particles' by Klebsiella pneumoniae. Microbiol. 143, 2521–2530.

Hörstmann, C., Brink, H.G., Chirwa, E.M.N., 2020. Pb (II) Bio-Removal, Viability, and Population Distribution of an Industrial Microbial Consortium: The Effect of Pb (II) and Nutrient Concentrations. Sustainability. 12, 2511. https://doi.org/10.3390/su12062511.

Jost, G., Martens-habbena, W., Pollehne, F., Schnetger, B., Labrenz, M., 2010. Anaerobic sulfur oxidation in the absence of nitrate dominates microbial chemoautotrophy beneath the pelagic chemocline of the eastern Gotland Basin, Baltic Sea. Fed. Eur. Microbiol. Soc. 71, 226–236. https://doi.org/10.1111/j.1574-6941.2009.00798.x

Karami, H., Ghasemi, M., Sara, M., 2013. Synthesis, Characterization and Application of Lead Sulfide Nanostructures as Ammonia Gas Sensing Agent. Int. J. Electrochem. Sci. 11661–11679.

Lombó, C.G., Posadas, Y., Quintanar, L., Eugenia, M., 2017. Neurotoxicity linked to dysfunctional metal ion homeostasis and xenobiotic metal exposure: Redox signaling and oxidative stress. Antioxidants Redox Signal. 1–114. https://doi.org/10.1089/ars.2017.7272.

Manecki, M., Bogucka, A., Bajda, T., Borkiewicz, O., 2006. Decrease of Pb bioavailability in solid by addition of phosphate ions. Environ. Chem. Lett. https://doi.org/10.1007/s10311-005-0030-1

Naik, M.M., Dubey, S.K., 2013. Ecotoxicology and Environmental Safety Lead resistant bacteria: Lead resistance mechanisms, their applications in lead bioremediation and biomonitoring. Ecotoxicol. Environ. Saf. 98, 1–7. https://doi.org/10.1016/j.ecoenv.2013.09.039.

Nassau, K., 1999. Energy bands. Britannica. https://www.britannica.com/science/color/additional-info#contributors (accessed 7.26.22).

National Cancer Institute, 2022. Definition of metabolic - NCI Dictionary of Cancer Terms - NCI. https://www.cancer.gov/publications/dictionaries/cancer-terms/def/metabolic (accessed 7.26.22).

Pan, X., Zhang, D., Fu, Q., 2012. Bioremediation of Pb-Contaminated Soil Based on Microbially Induced Calcite Precipitation. J. Microbiol. Biotechnol. 22, 244–247.

Ramkumar, T., Selvakumar, M., Vasanthsankar, R., Sathishkumar, A.S., Narayanasamy, P., Girija, G., 2018. Rietveld refinement of powder X-ray diffraction, microstructural and mechanical studies of magnesium matrix composites processed by high energy ball milling. J. Magnes. Alloy. 6, 390–398. https://doi.org/10.1016/j.jma.2018.08.002.

Rigoletto, M., Calza, P., Gaggero, E., Malandrino, M., Fabbri, D., 2020. Bioremediation Methods for the Recovery of Lead-Contaminated Soils: A Review. Appl. Sci. 10,3528/ https://doi:10.3390/app10103528.

Rodríguez-Carvajal, J., 1993. Recent advances in magnetic structure determination by neutron powder diffraction. Phys. B Phys. Condens. Matter 192, 55–69. https://doi.org/10.1016/0921-4526(93)90108.

Sevak, P.I., Pushkar, B.K., Kapadne, P.N., 2021. Lead pollution and bacterial bioremediation: a review. Environ. Chem. Lett. https://doi.org/10.1007/s10311-021-01296-7.

Statista, 2019. Lead reserves worldwide as of 2018, by country (in million metric tons). Chem. Resour. https://www.statista.com/statistics/273652/global-lead-reserves-by-selected-countries/ 2/5 (accessed 5.2.20).

Stutzman, P.E., Feng, P., Bullard, J.W., 2016. Phase Analysis of Portland Cement by Combined Quantitative X-Ray Powder Diffraction and Scanning Electron. J. Res. Natl. Inst. stndards Technol. 121, 47–107. https://doi.org/10.6028/jres.121.004.

Tao, Y., Zhang, C., Lü, T., 2020. Removal of Pb (II) Ions from Wastewater by Using Magnetic Nanoparticles. Appl. Sci. 10, 948. https://dio.org/10.3390/app10030948.

Tiquia-arashiro, S.M., 2018. Lead absorption mechanisms in bacteria as strategies for lead bioremediation. Appl. Microbiol. Biotechnol. 102, 5437–5444.

Topolska, J., Latowski, D., Kaschabek, S., Manecki, M., Merkel, B.J., Rakovan, J., 2013. Pb remobilization by bacterially mediated dissolution of pyromorphite $Pb_5(PO_4)_3Cl$ in presence of phosphate-solubilizing Pseudomonas putida. Environ. Sci. Pollut. Res. 5. https://doi.org/10.1007/s11356-013-1968-3.

Veenhuyzen, B. Van, Chirwa, E.M.N., Brink, H.G., 2021. Microbial Pb(II) Precipitation: the Role of Biosorption as a Pb(II) Removal Mechanism. Chem. Eng. Trans. 86, 181–185. https://doi.org/10.3303/CET2186031.

Walczak, A.B., Kafantaris, F.C.A., Druschel, G.K., Yee, N., Young, L.Y., 2016. Transformation of galena to pyromorphite produces bioavailable sulfur for neutrophilic chemoautotrophy. Gebiology. 0, 1–8. https://doi.org/10.1111/gbi.12199.

Wang, H., Cheng, H., Wang, F., Wei, D., Wang, X., 2010. An improved 3-(4,5-dimethylthiazol-2-yl)-2,5-diphenyl tetrazolium bromide (MTT) reduction assay for evaluating the viability of Escherichia coli cells. J. Microbiol. Methods 82, 330–333. https://doi.org/10.1016/j.mimet.2010.06.014.

Zhang, H., Zhao, Z., Chen, S., Kang, P., Wang, Yue, Feng, J., Jia, J., Yan, M., Wang, Yan, Xu, L., 2018. Paracoccus versutus KS293 adaptation to aerobic and anaerobic denitrification: Insights from nitrogen removal, functional gene abundance, and proteomic profiling analysis. Bioresour. Technol. 260, 321–328. https://doi.org/10.1016/j.biortech.2018.03.123.

Zhang, X., Yang, L., Li, Y., Li, H., Wang, W., Ye, B., 2012. Impacts of lead / zinc mining and smelting on the environment and human health in China. Environ. Monit. Assess. 2261–2273. https://doi.org/10.1007/s10661-011-2115-6.